

RESEARCH ARTICLE | JANUARY 28 2016


A full-field transmission x-ray microscope for time-resolved imaging of magnetic nanostructures

J. Ewald; P. Wessels; M. Wieland; T. Nisius; A. Vogel; G. Abbati; S. Baumbach; J. Overbuschmann; J. Viefhaus; G. Meier; T. Wilhein; M. Drescher


AIP Conf. Proc. 1696, 020005 (2016)

<https://doi.org/10.1063/1.4937499>







Nanotechnology & Materials Science




Optics & Photonics



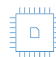
Impedance Analysis




Scanning Probe Microscopy



Sensors




Failure Analysis & Semiconductors



Unlock the Full Spectrum.
From DC to 8.5 GHz.
Your Application. Measured.

[Find out more](#)



A full-field transmission X-ray microscope for time-resolved imaging of magnetic nanostructures

J. Ewald*, P. Wessels^{†,**}, M. Wieland^{†,**}, T. Nisius*, A. Vogel[‡], G. Abbati*, S. Baumbach*, J. Overbuschmann*, J. Viefhaus[§], G. Meier^{†,¶}, T. Wilhein* and M. Drescher^{†,**}

*Institute for X-Optics (IXO), Hochschule Koblenz, Joseph-Rovan-Allee 2, 53424 Remagen, Germany

[†]The Hamburg Centre for Ultrafast Imaging (CUI), University of Hamburg, Luruper Chaussee 149, 22761 Hamburg, Germany

**Institut für Experimentalphysik, University of Hamburg, Luruper Chaussee 149, 22761 Hamburg, Germany

[‡]Institut für Angewandte Physik, University of Hamburg, Jungiusstraße 11, 20355 Hamburg, Germany

[§]Deutsches Elektronen-Synchrotron (DESY), Notkestraße 85, 22607 Hamburg, Germany

[¶]Max Planck Institute for the Structure and Dynamics of Matter, Luruper Chaussee 149, 22761 Hamburg, Germany

Abstract. Sub-nanosecond magnetization dynamics of small permalloy ($\text{Ni}_{80}\text{Fe}_{20}$) elements has been investigated with a new full-field transmission microscope at the soft X-ray beamline P04 of the high brilliance synchrotron radiation source PETRA III. The soft X-ray microscope generates a flat-top illumination field of $20\ \mu\text{m}$ diameter using a grating condenser. A tilted nanostructured magnetic sample can be excited by a picosecond electric current pulse via a coplanar waveguide. The transmitted light of the sample plane is directly imaged by a micro zone plate with $< 65\ \text{nm}$ resolution onto a 2D gateable X-ray detector to select one particular bunch in the storage ring that probes the time evolution of the dynamic information successively via XMCD spectromicroscopy in a pump-probe scheme. In the experiments it was possible to generate a homogeneously magnetized state in patterned magnetic layers by a strong magnetic Oersted field pulse of 200 ps duration and directly observe the recovery to the initial flux-closure vortex patterns.

Keywords: magnetization dynamics, magnetic vortices, X-ray microscopy, time-resolved imaging

PACS: 75.78.Fg, 78.47.da, 75.70.Kw, 68.37.Yz

INTRODUCTION

The study of nanoscale magnetic systems at its fundamental timescales is motivated by future applications in modern data storage technology considering improvement of data density as well as access time and stability. This requires the ability to conduct time-resolved measurements with high resolution in the soft X-ray regime utilizing the X-ray magnetic circular dichroism (XMCD) [1, 2]. For this purpose a full-field transmission X-ray microscope with the ability to pump and probe magnetic permalloy structures was developed [3, 4, 5]. It enables the direct observation of magnetization relaxation from nonequilibrium states subsequent to the application of a strong Oersted field pulse. For time-resolved measurements, the microscope features a fast gateable X-ray detector which is capable of selecting one particular bunch in the storage ring that probes the time evolution after the initial field pulse.

EXPERIMENTAL SETUP

Mobile X-ray microscopy endstation for P04

The microscope endstation for the soft X-ray beamline P04 at PETRA III consists of a rail-system which accepts up to three standardized, interchangeable vacuum chambers. One of these is outfitted with four three-axis piezo stages to mount the optics and additional components for the full-field X-ray microscope setup. The radiation delivered by the P04 beamline is focused by a grating condenser optic of 1 mm diameter into a $20\ \mu\text{m}$ diameter illumination spot. The focal length is $f_c = 34\ \text{mm}$ at 852 eV photon energy. The deflected radiation from each grating overlaps in the focal plane to form a homogeneous illumination profile [6]. A micro zone plate of $80\ \mu\text{m}$ diameter with an outermost zone

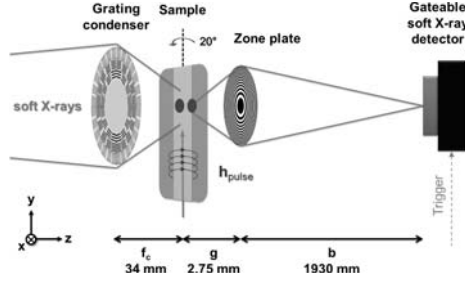


FIGURE 1: Schematic setup of the full-field transmission X-ray microscope. A grating condenser with gold central stop focuses the X-ray beam on the sample mounted at an angle with respect to the photon direction. The micro zone plate with 50 nm outermost zone width images the sample onto the gateable detector. Electric pulses through a conducting waveguide are used to excite the sample [3].

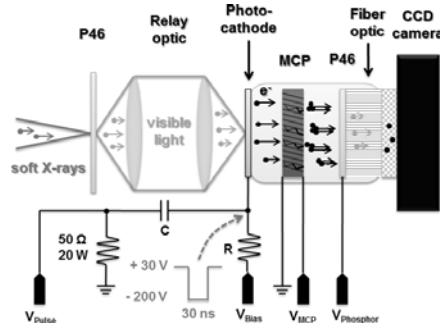


FIGURE 2: Schematic setup of the fast gateable X-ray detector. The microscope image is projected on a P46 phosphor screen and imaged by a relay optic onto an image intensifier. The detector can be opened by applying a negative bias voltage to the photocathode synchronized with X-ray pulses by using the storage ring trigger supplied by the beamline. The light output from the second P46 phosphor is collected by a CCD camera [7].

width of 50 nm and matched numerical aperture to the condenser is used for the imaging. The microscope image can be recorded by a back-thinned CCD camera or, for time-resolved imaging, by a fast gateable X-ray detector. In order to acquire dynamic images, the magnetic sample is excited by a short magnetic field pulse emerging from current pulses in the conductor of a waveguide with 186 ps pulse duration and < 130 ps residual jitter. To access the in-plane magnetization component, the sample-plane normal is tilted by 20° with respect to the photon beam direction. The magnetic response is probed by a soft X-ray pulse in the microscope. In the time-resolved mode of PETRA III 40 bunches are circulating in the ring with a separation of 192 ns. Due to the high pulse peak amplitude, the picosecond pulse generator for excitation of the sample is operated at the roundtrip frequency of the synchrotron of 130.1 kHz. Therefore, 39 of the 40 bunches can not be used for the pump-probe experiment and have to be blocked. This is done by an in-house developed gated detector shown in figure 2.

Fast gateable X-ray detector for time-resolved imaging at P04

The microscope image is projected onto a P46 phosphor screen and imaged via a relay optic consisting of two fast camera lenses onto the photocathode of a commercial third generation image intensifier. The intensifier features a single microchannel plate (MCP) amplification stage and a P46 output screen that is fiber-coupled to a Princeton Instruments PIXIS-XF back-illuminated charge-coupled device (CCD) camera with 1024×1024 pixel of $13 \mu\text{m}$ size. By applying a positive bias voltage of +30 V onto the photocathode of the image intensifier, the detector is closed by default as the generated negatively charged electrons can not leave the cathode surface. A 30 - 40 ns long negative voltage gate pulse of -200 V amplitude synchronized to the storage ring trigger opens the detector to pass on the image information of the desired bunch by acceleration of the photoelectrons onto the MCP. The light output of the phosphor screen is collected at a fixed pump-probe delay Δt and integrated on the camera chip. The temporal overlap between pump, probe and gate pulses is achieved by moving a fast photodiode into the soft X-ray beam and monitoring all trigger signals with a broadband scope by carefully taking into account electronic signal delays in cables and equipment. Figure 3 shows the results from commissioning the fast gateable X-ray detector at the P04 beamline. By tuning the delay with respect to the storage ring trigger, the photon pulses of the beamline convoluted with the afterglow of the screens and the photocathode gate pulse duration of 40 ns become visible. The afterglow is minimized by using a fast-decay phosphor (P46) to minimize ghost imaging from a previous frame [8]. Typically, the detector is operated at 5.4 kV MCP to phosphor voltage, 600 V MCP and 170 V photocathode voltage. The pulse duration of 40 ns was chosen because it is short enough to select the signal from only one bunch and further increase does not

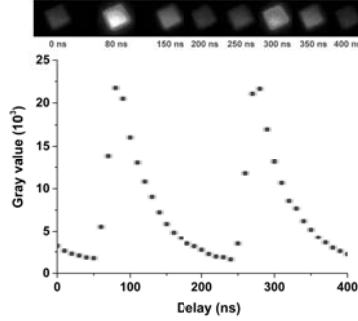


FIGURE 3: Brightness of a silicon nitride membrane shadow image (top) coated with a permalloy layer with respect to the detector-gate pulse delay (bottom). The 192 ns separation of the 40 bunches in the storage ring convoluted with the gate pulse duration of 40 ns and the phosphor (P46) decaytime is observable [7].

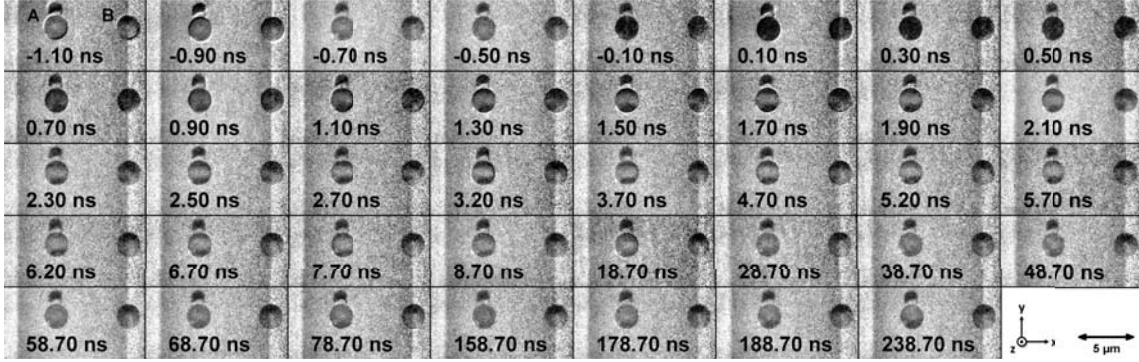


FIGURE 4. Image sequence showing the domain pattern recovery of 2 μm diameter permalloy discs (A and B) excited by the magnetic field of a current pulse. The 186 ps long pulse with 82 mT peak amplitude at $\Delta t = 0$ ns aligns the magnetization of the microdiscs in overlap with the waveguide conductor along the x direction. The black spot on top of circle A is residue of a non-magnetic material from the fabrication process [7].

result in considerably more counts in the camera.

RESULTS AND DISCUSSION

Circular permalloy ($\text{Ni}_{80}\text{Fe}_{20}$) elements were investigated for their dynamic response to an excitation pulse. These 30 nm thick patterns of 2 μm diameter were prepared by electron-beam lithography and physical vapor deposition. The structures exhibit a vortex state with a continuous in-plane magnetization rotation around a out-of-plane core in the center. One circle is positioned in complete (A) and one in partial overlap (B) to the waveguide as can be seen in figure 4. Here the dark areas represent an alignment in the x -direction. The coplanar waveguide (CPW) is formed by a 300 nm thick copper layer on top of the sample. An 186 ps long excitation pulse with 130 V peak amplitude launched into the 100 Ω waveguide with a conductor of 10 μm width corresponding to a field of 82 mT on the conductor surface. Circle A is forced into a uniformly magnetized state with a net magnetization pointing along the x -axis. The magnetization then rapidly decays into a state with two domains in the top and bottom aligned in opposite direction to the central part which remains stable for 10 ns with minor changes. Afterwards, the homogenous gray level of the disc indicates a random, not reproducible dynamic behavior. Also before the current pulse a similar, non distinct, vortex state hints towards an indefinite final state. An equal probability for both final chiralities defining the sense of rotation of the vortex might explain the gray shape when the black contrast appears alternately in the top and in the bottom sector. The partially overlapping disc B in figure 4 ends up in a vortex with stable chirality after already 6 ns without the indefinite state occurring at circle A. The different behavior of the two cases originates from the spatially dependent field configuration mainly due to a differing M_z component. The field in x direction to the current flow experienced by disc A is more homogeneous compared to the case at the conductor boundary where circle B is located. Here, the x component only partly acts on the magnetization of the disc due to the limited overlap and the amplitude may vary from

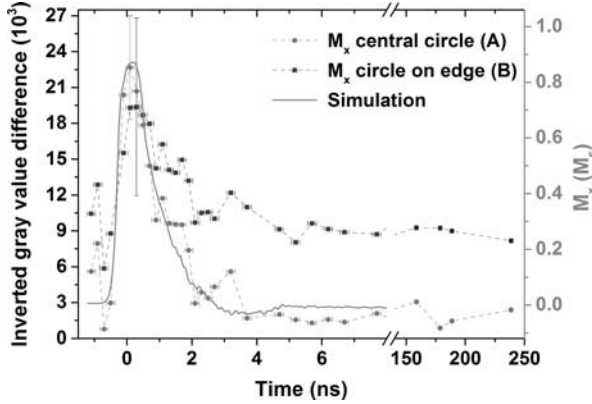


FIGURE 5: Gray value of the XMCD contrast images for circle (A) and (B) in figure 4 corresponding to the magnetization component M_x in the permalloy discs on the CPW conductor investigated in the delay scans. Finite-element-based simulations for the circle (A) are also shown [3, 7].

the center to the edges due to the skin effect. Finite-element-based micromagnetic simulations of the magnetization response are shown in comparison with measured data in figure 5 [9, 10]. Compared to experiments and simulations on the dynamic response of $2\ \mu\text{m}$ magnetic permalloy squares [3], the circular patterns decay more rapidly due to the absence of domain wall boundaries.

SUMMARY AND OUTLOOK

We have set up a new full-field transmission X-ray microscope with sub-100 nm spatial resolution and a fast gateable detector for time-resolved measurements with subnanosecond temporal resolution. This instrument enabled us to directly observe the dynamic domain pattern destruction and recovery of magnetic permalloy disks.

ACKNOWLEDGMENTS

The authors would like to thank Pambos Charalambous (ZonePlates.com) for manufacturing of zone plate and grating condenser. Parts of this research were carried out at the light source PETRA III at DESY, a member of the Helmholtz Association (HGF). We would like to thank Leif Glaser, Jörn Seltmann, and Frank Scholz for assistance in using beamline P04. Financial support from the Deutsche Forschungsgemeinschaft (DFG) via the Sonderforschungsbereich 668 and the excellence cluster 'The Hamburg Centre for Ultrafast Imaging' (CUI) is gratefully acknowledged. Additionally, we thank the Bundesministerium für Bildung und Forschung (BMBF) for funding through the Forschungsschwerpunkt 301 (05KS7GU4 and 05KS7UL1).

REFERENCES

1. G. Schütz, W. Wagner, W. Wilhelm, P. Kienle, R. Zeller, R. Frahm, and G. Materlik, *Phys. Rev. Lett.* **58**, 737 (1987).
2. P. Fischer, *Curr. Opin. Solid State Mater. Sci.* **7**, 173 (2003).
3. P. Wessels, J. Ewald, M. Wieland, T. Nisius, A. Vogel, J. Viefhaus, G. Meier, T. Wilhein, and M. Drescher, *Phys. Rev. B* **90**, 184417 (2014).
4. P. Wessels, M. Schlie, M. Wieland, J. Ewald, G. Abbati, S. Baumbach, J. Overbuschmann, T. Nisius, A. Vogel, A. Neumann, et al., *J. Phys. Conf. Ser.* **463**, 012023 (2013).
5. P. Wessels, J. Ewald, M. Wieland, T. Nisius, G. Abbati, S. Baumbach, J. Overbuschmann, A. Vogel, A. Neumann, J. Viefhaus, et al., *J. Phys. Conf. Ser.* **499**, 012009 (2014).
6. U. Vogt, M. Lindblom, P. Charalambous, B. Kaulich, and T. Wilhein, *Opt. Lett.* **31**, 1465 (2006).
7. P. Wessels, *Time-resolved imaging of magnetic nanostructures in the visible and soft X-ray spectral range*, Ph.D. thesis, University of Hamburg (2014).
8. P. Hoess, and K. Fleder, *Proc. SPIE* **4183**, 127 (2001).
9. T. Fischbacher, M. Franchin, G. Bordignon, and H. Fangohr, *IEEE Trans. Magn.* **43**, 2896 (2007).
10. H. Fangohr, T. Fischbacher, M. Franchin, G. Bordignon, J. Generowicz, A. Knittel, and M. Walter, *NMAG User Manual, Release 0.2.1*, University of Southampton, Highfield, Southampton SO17 1BJ, United Kingdom, 2012.